From Illumination to Prediction: A Kinetic Model for Photoredox Catalytic Activity

Ádám Madarász*[a], Péter Pál Fehér*[a] and András Stirling*[a,b]
[a]Institute of Organic Chemistry, HUN-REN Research Centre for Natural Sciences, Budapest, Hungary
[b]Eszterházy Károly Catholic University, Eger, Hungary

Supplementary Information

Table of Contents

1.	Detailed derivation of the equations employed in the simulations	S2-S7
1.1.	The full kinetic model for the oxidative quenching	S2
1.2.	The full kinetic model for the reductive quenching	S4
1.3.	Defining the diffusion-controlled regime	S5
1.4.	Estimation of the volumetric photon radiation	S5
1.5.	Derivation of the rate of photon absorption	S6
1.6.	The inequality between the standard reduction potentials of P and Q for oxidation	S6
1.7.	The inequality between the standard reduction potentials of P and Q for reduction	S7
2.	Details of the implementation of diffusion control	S8
3.	Derivation of Equation 3b (unproductive quenching)	S9
4.	Details of the kinetic simulations of the $[Ru(bpy)_3]^{2+}$ + TTA system	S11
5.	References	S12
6.	Additional figures	S13-S23
6.1.	**Fig. S2.** Nonlinear dependence of the activation barrier on λ and ΔG_0	S13
6.2.	**Figs. S3-S4.** Convergence of the kinetic simulations	S14
6.3.	**Fig. S5.** Steady-state rates	S16
6.4.	**Figs. S6-S7.** Distribution of the steady-state concentrations	S17
6.5.	**Fig. S8.** Distribution of E_Q for different reorganization energies	S19
6.6.	**Fig. S9.** Distribution of E_Q for different lamp intensities	S20
6.7.	**Fig. S10.** Distribution of E_Q for different effective absorption coefficients	S21
6.8.	**Fig. S11.** Distribution of E_Q for different excitation lifetimes	S22
6.9.	**Figs. S12-S13.** Distribution of E_Q for different diffusion rates	S23

1. Detailed derivation of the equations employed in the simulations

1.1. The elementary steps and the full kinetic model for the oxidative quenching

The photochemical excitation is given by the following equation:

$$\mathbf{PC} \underset{k_2}{\overset{h\nu}{\rightleftharpoons}} \mathbf{PC}^* \qquad (1)$$

where $h\nu$ indicates the light absorption and k_2 is the rate coefficient of the relaxation of the excited state. As we discussed in the main text, the light absorption process can be described by rate coefficient k_1.

The electron transfer (ET) between the photocatalyst (**PC**) and a quencher (**Q**) can be formulated as:

$$\mathbf{PC} + \mathbf{Q} \underset{k_4}{\overset{k_3}{\rightleftharpoons}} \mathbf{PC}^+ + \mathbf{Q}^- \qquad (2)$$

where k_3 and k_4 are the rate constants of the forward and backward reactions. For this process the backward route is responsible for the annihilation of the reduced quencher.

The excited state photocatalyst (**PC***) can also reduce the quencher:

$$\mathbf{PC}^* + \mathbf{Q} \underset{\phi_{ce}k_6}{\overset{\phi_{ce}k_5}{\rightleftharpoons}} \mathbf{PC}^+ + \mathbf{Q}^- \qquad (3)$$

where k_5 and k_6 are the rate coefficients of the forward and backward reactions. The forward route of this equilibrium is the main source of the reduced $\mathbf{Q}^-$.

The unproductive geminal quenching within a cage can be described with an effective, irreversible reaction equation:

$$\mathbf{PC}^* + \mathbf{Q} \xrightarrow{(1-\phi_{ce})k_5} \mathbf{PC} + \mathbf{Q} \qquad (4)$$

The corresponding rate equations:

$$\frac{d[PC]}{dt} = -k_1[PC] + k_2[PC^*] - k_3[PC][Q] + k_4[PC^+][Q^-] + (1-\phi_{ce})k_5[PC^*][Q] \qquad (5)$$

$$\frac{d[PC^+]}{dt} = \frac{d[Q^-]}{dt} = k_3[PC][Q] - k_4[PC^+][Q^-] + \phi_{ce}k_5[PC^*][Q] - \phi_{ce}k_6[PC^+][Q^-] \qquad (6)$$

$$\frac{d[PC^*]}{dt} = -\frac{d[PC]}{dt} - \frac{d[PC^+]}{dt} = k_1[PC] - k_2[PC^*] - \phi_{ce}k_5[PC^*][Q] + \phi_{ce}k_6[PC^+][Q^-] - (1-\phi_{ce})k_5[PC^*][Q] \qquad (7)$$

Eq. 7 is not independent but follows from Eqs. 5 and 6. On the other hand, conservation of matter for the photocatalyst provides an independent equation:

$$[PC]_0 + [PC^+]_0 + [PC^*]_0 = [PC] + [PC^+] + [PC^*] \qquad (8)$$

The zero subscript denotes initial concentrations.

Conservation of matter for the quencher:

$$[Q]_0 + [Q^-]_0 = [Q] + [Q^-] \qquad (9)$$

The time dependence of [**Q**] follows from Eqs. 6 and 9.

Conservation of charge:

$$[PC^+]_0 - [Q^-]_0 = [PC^+] - [Q^-] \qquad (10)$$

Given the initial concentrations and the rate coefficients, the rate equations (eqs. 5-10) can be integrated numerically and the time evolution of the concentrations can be obtained. We used the COPASI software for that.[1] Equilibrium concentrations are reached when eqs. 5-7 become zero. The equilibrium concentration of the reduced quencher characterizes the performance of the photocatalyst.

The rate coefficients can be obtained from the free energy barrier of the actual elementary steps. In particular, the rate coefficients for electron transfers are determined by employing the Marcus theory[2]: the activation energy of the electron transfer $(\Delta G^{\ddagger})$ can be estimated from the free energy change (ΔG°) of the electron transfer and the reorganization energy λ of the system:

$$\Delta G^{\ddagger} = \frac{(\lambda + \Delta G^{\circ})^2}{4\lambda} \qquad (11)$$

Here we assume that the reorganization energy originates mainly from the solvent and depends strongly on its polarity. It can vary from 25 kJ/mol up to 200 kJ/mol.[3–6] In the first simulations we used 54.5 kJ/mol (13.0 kcal/mol, 0.56 eV) for the reorganization energies. From the activation energy $\Delta G^{\ddagger}$ of the electron transfer the rate constant can be obtained using the Eyring equation of transition state theory (TST) for uni- and bimolecular reactions, respectively:

$$k = \frac{k_B T}{h} exp\left(-\frac{\Delta G^{\ddagger}}{RT}\right) \qquad (12a)$$

$$k = \frac{k_B T}{hc^{\ominus}} exp\left(-\frac{\Delta G^{\ddagger}}{RT}\right) \qquad (12b)$$

where k_B and h are the Boltzmann and Planck constants, respectively, R is the universal gas constant, T is the temperature and $c^{\ominus}$ is the standard concentration (1.0 mol/l). Note that there is an upper limit for the rate constants, namely the diffusion limit in solutions, typically 10^{10} dm^3/mol/s. For the actual diffusion rate an activation free energy ΔG_D can be derived by Eq. 12. To prevent faster reactions in the simulations all bimolecular rate coefficient is constrained not to be higher than the diffusion rate. This can be achieved by increasing the corresponding barrier to reach ΔG_D and take into account this increase for the opposite direction as well (see the implementation later). This implies that the reaction free energy (i.e.. difference of the activation energies for the back-and-forth directions) does not change.

We note that the form for the rate of electron transfer more often invoked is:[7]

$$k = \frac{2\pi}{\hbar}|V^2|\frac{1}{\sqrt{4\pi\lambda k_B T}} exp\left(-\frac{\Delta G^{\ddagger}}{RT}\right) \qquad (12')$$

where V is the electronic coupling between the initial and final states. In our model we assume i) the validity of the classical TST, when the preexponential factor is independent of the electron tunneling possibility and ii) that the formula obtaining $\Delta G^{\ddagger}$ (Eq. 11), to a good approximation, remains valid in both the adiabatic and non-adiabatic limits; i.e. we assume the validity of Eqs. 12a and b. We also note that the variation of the exponential is typically order of magnitudes larger than the difference between the preexponentials in equations 12a, 12b and 12', therefore the choice has limited effect on the final results.

1.2. Derivation of the kinetic model for reductive quenching, the analogous equations:

The photochemical excitation is given by the following equation:

$$\mathbf{PC} \underset{k_2}{\overset{h\nu}{\rightleftharpoons}} \mathbf{PC}^* \qquad (1')$$

where $h\nu$ indicates the light absorption and k_2 is the rate coefficient of the relaxation of the excited state. As we discussed in the main text, the light absorption process can be described by rate coefficient k_1.

The electron transfer (ET) between the photocatalyst (**PC**) and a quencher (**Q**) can be formulated as:

$$\mathbf{PC} + \mathbf{Q} \underset{k_4'}{\overset{k_3'}{\rightleftharpoons}} \mathbf{PC}^- + \mathbf{Q}^+ \qquad (2')$$

where k_3' and k_4' are the rate constants of the forward and backward reactions. For this process the backward route is responsible for the annihilation of the reduced quencher.

The excited state photocatalyst (**PC***) can also oxidize the quencher:

$$\mathbf{PC}^* + \mathbf{Q} \underset{\phi_{ce}k_6'}{\overset{\phi_{ce}k_5'}{\rightleftharpoons}} \mathbf{PC}^- + \mathbf{Q}^+ \qquad (3')$$

where k_5' and k_6' are the rate coefficients of the forward and backward reactions. The forward route of this equilibrium is the main source of the reduced $\mathbf{Q}^-$.

$$\mathbf{PC}^* + \mathbf{Q} \xrightarrow{(1-\phi_{ce})k_5} \mathbf{PC} + \mathbf{Q} \qquad (4')$$

Eq. 4' is the equation of the irreversible unproductive quenching reaction.

The corresponding rate equations:

$$\frac{d[PC]}{dt} = -k_1[PC] + k_2[PC^*] - k_3'[PC][Q] + k_4'[PC^-][Q^+] + (1-\phi_{ce})k_5'[PC^*][Q] \qquad (5')$$

$$\frac{d[PC^-]}{dt} = \frac{d[Q^+]}{dt} = k_3'[PC][Q] - k_4'[PC^-][Q^+] + \phi_{ce}k_5'[PC^*][Q] - \phi_{ce}k_6'[PC^-][Q^+] \qquad (6')$$

$$\frac{d[PC^*]}{dt} = -\frac{d[PC]}{dt} - \frac{d[PC^+]}{dt} = k_1[PC] - k_2[PC^*] - \phi_{ce}k_5'[PC^*][Q] + \phi_{ce}k_6'[PC^-][Q^+] - (1-\phi_{ce})k_5'[PC^*][Q] \qquad (7')$$

Conservation of matter for the photocatalyst provides an independent equation, where the zero subscript denotes initial concentrations:

$$[PC]_0 + [PC^-]_0 + [PC^*]_0 = [PC] + [PC^-] + [PC^*] \qquad (8')$$

Conservation of matter for the quencher:

$$[Q]_0 + [Q^+]_0 = [Q] + [Q^+] \qquad (9')$$

The time dependence of [**Q**] follows from eqs. 6' and 9'.

Conservation of charge:

$$[PC^-]_0 - [Q^+]_0 = [PC^-] - [Q^+] \qquad (10')$$

1.3. Defining the diffusion-controlled regime by electromotive force range

The range of $\Delta G^{\ominus}$, and thus the range of standard reduction potentials can be given as a function of the TST barrier of the diffusion control limit and the reorganization energy λ. For this we have seek the $\Delta G^{\ominus}$ values for which the barrier from the Marcus equation matches the diffusion control barrier ΔG_D:

$$\Delta G_D = \frac{(\lambda + \Delta G^{\ominus})^2}{4\lambda} \qquad (13)$$

Equation 13 has two solutions: $\Delta G_1^{\ominus} = 2\sqrt{\Delta G_D \lambda} - \lambda$ and $\Delta G_2^{\ominus} = -2\sqrt{\Delta G_D \lambda} - \lambda$. Therefore, the range of $\Delta G^{\ominus}$ values where diffusion control prevails is

$$\Delta G_1^{\ominus} - \Delta G_2^{\ominus} = 4\sqrt{\Delta G_D \lambda} \qquad (14)$$

This implies that for larger reorganization energies the diffusion-controlled ET range is wider. Using the relation between the electromotive force of a cell and the free energy of the cell reaction: $\Delta G_{cell}^0 = -zFE_{cell}^0$, we obtain:

$$4\sqrt{\Delta G_D \lambda} = zF\left(E_2^{\ominus} - E_1^{\ominus}\right) \qquad (15)$$

1.4. Estimation of the volumetric photon radiation

In Eqs. 5 and 7 the contribution of **PC** to the formation rate of **PC*** is expressed formally with k_1[**PC**]. However, the dependence of this rate on [**PC**] is not as simple, because the light absorption depends on several factors. The effect of light can be incorporated into the model in the following way: The spectrum of the lamp can be characterized by the light intensity distribution as a function of the frequency ν: $P_{lamp}(\nu)$. The total power of the light source is obtained by $\int_0^{\infty} P_{lamp}(\nu)d\nu$. The volumetric photon radiation (i.e., number of photons measured in moles per unit area per unit time arriving at volume V) in the dimension of mol/volume/time:

$$I_{photon} = \int_0^{\infty} \frac{P_{lamp}(\nu)}{VN_A h\nu} d\nu = \frac{1}{VN_A} \int_0^{\infty} \frac{P_{lamp}(\nu)}{h\nu} d\nu \qquad (16)$$

where N_A is the Avogadro constant and $\frac{P_{lamp}(\nu)}{h\nu} d\nu$ is the number of photons within a $d\nu$ interval around frequency ν. For example, if the reaction volume V is 2 ml and the wavelength of a monochromatic light is 450 nm with an effective power of 30 W then the volumetric photon radiation is:

$$I_{photon} \approx 0.0564 \frac{mol}{dm^3\, s} \qquad (17)$$

Note that the effective power of the lamp is usually smaller within the whole spectrum due to the limitations of the experimental setup. We need to use the volumetric molar photon radiation, because we use concentrations (i.e., the analogue volumetric quantity for matter).

1.5. Derivation of the rate of photon absorption

According to the Beer–Lambert law we can estimate the quantity of the absorbed photons within unit time in *mol/volume* ie. concentration units:

$$I_{absorbed} = I_{photon} - I_{transmitted} = \int_0^{\infty} \frac{P_{lamp}(\nu)}{VN_A h\nu}\left(1 - 10^{-\varepsilon(\nu)[PC]l}\right)d\nu \qquad (18)$$

where l is the optical path length (in this study it is 1 cm), and $\varepsilon(\nu)$ is the molar absorption coefficient. Note that expression $10^{-\varepsilon(\nu)[PC]l}$ corresponds to the ratio of the transmitted light as dictated by the Beer-Lambert law. We note that $I_{absorbed}$ is equal to the concentration of **PC*** generated within unit time from the actual [**PC**], i.e., the rate of production of **PC*** from **PC** by light. The integral in eq. 18 is too complicated to perform in each time-step. For a simpler equation the following considerations can be done:

i) the initial absorbance $I^{0}_{absorbed}$ can be defined analogously:

$$I^{0}_{absorbed} = \int_0^{\infty} \frac{P_{lamp}(\nu)}{VN_A h\nu}\left(1 - 10^{-\varepsilon(\nu)[PC]_0 l}\right)d\nu \qquad (19)$$

ii) then we can define the mean or effective absorption coefficient $\bar{\varepsilon}$ which effectively characterizes the overlap between the spectrum of the light source and the absorption spectrum:

$$\bar{\varepsilon} = -\frac{log_{10}\left(\frac{I_{photon} - I^{0}_{absorbed}}{I_{photon}}\right)}{[PC]_0 l} \qquad (20)$$

If the actual concentration of the photocatalyst does not change too much as compared to the initial concentration, then the absorbed photon flux can be estimated by the next equation.

$$I_{absorbed} \approx I_{photon}\left(1 - 10^{-\bar{\varepsilon}[PC]l}\right) \qquad (21)$$

In this study Eqs. 20 and 21 are employed.

1.6. Derivation of the inequality expression between the standard reduction potentials of P and Q for oxidative quenching:

We assume that at most 1‰ [$\mathbf{Q}^-$] is present when **PC** and **Q** are together without light. This implies the following concentration ratios: $[Q^-]/[Q] = 0.001/0.999 = 0.001$; and $[PC^+]/[PC] = 0.001/0.999 = 0.001$.

We therefore require that the equilibrium constant characterizing the ET between **P** and **Q** cannot be larger than that corresponding to 1‰ [$\mathbf{Q}^-$]:

$$K = \frac{[Q^-][PC^+]}{[Q][PC]} \leq \frac{0.001 \cdot 0.001}{0.999 \cdot 0.999} \cong 10^{-6}$$

Using the relation between the equilibrium constants and electromotive forces we can obtain the required expression:

$$RT \cdot \ln K = zFE^{0}_{cell} = zF\left(E^{0}_{Q} - E^{0}_{PC}\right)$$

$$RT \cdot ln\left(\frac{[Q^-][PC^+]}{[Q][PC]}\right) \leq RT \cdot ln\left(\frac{0.001 \cdot 0.001}{0.999 \cdot 0.999}\right) \cong RT \cdot ln\left(10^{-6}\right)$$

$$E^{0}_{Q} - E^{0}_{PC} \leq \frac{RT}{zF} \cdot \ln\left(10^{-6}\right) = -0.35V$$

$E_{PC}^{0} \geq E_{Q}^{0} + 0.35V$

We note that for a less stringent condition of 1% [**Q**⁻] we obtain: $E_{PC}^{0} \geq E_{Q}^{0} + 0.24V$.

1.7. Derivation of the inequality expression between the standard reduction potentials of P and Q for reductive quenching:

We assume that at most 1‰ [**Q**⁺] is present when **PC** and **Q** are together without light. This implies the following concentration ratios: $[Q^+]/[Q] = 0.001/0.999 = 0.001$; and $[PC^-]/[PC] = 0.001/0.999 = 0.001$.
We therefore require that the equilibrium constant characterizing the ET between **P** and **Q** cannot be larger than that corresponding to 1 ‰ [**Q**⁻]:

$$K = \frac{[Q^+][PC^-]}{[Q][PC]} \leq \frac{0.001 \cdot 0.001}{0.999 \cdot 0.999} \cong 10^{-6}$$

Using the relation between the equilibrium constants and electromotive forces we can obtain the required expression:

$$RT \cdot \ln K = zFE_{cell}^{0} = zF\left(E_{PC}^{0} - E_{Q}^{0}\right)$$

$$RT \cdot ln\left(\frac{[Q^+][PC^-]}{[Q][PC]}\right) \leq RT \cdot ln\left(\frac{0.001 \cdot 0.001}{0.999 \cdot 0.999}\right) \cong RT \cdot ln\left(10^{-6}\right)$$

$$E_{PC}^{0} - E_{Q}^{0} \leq \frac{RT}{zF} \cdot \ln\left(10^{-6}\right) = -0.35V$$

$$E_{PC}^{0} \leq E_{Q}^{0} - 0.35V$$

We note that for a less stringent condition of 1% [**Q**⁺] we obtain: $E_{PC}^{0} \leq E_{Q}^{0} - 0.24V$.

2. Details of the implementation of diffusion control

To handle correctly the issues arising from the diffusion control for each reaction, we have to consider the barriers of both the forward and reverse steps simultaneously and treat the following two conditions:

a) if the smaller of the two activation energies is lower than the activation energy associated with diffusion ($^{\Delta G_D}$), then it has to be increased to reach $^{\Delta G_D}$;
b) if $^{\Delta G^{\ddagger}}$ of a given step is increased, then the barrier of the opposite step has to be also increased with the same amount in order to keep the reaction energy unchanged (the difference of the two barriers has to be equal to the reaction energy).

Actual implementation in our simulation for an arbitrary reversible reaction, where the forward barrier is $^{\Delta G_{1,orig}^{\ddagger}}$ and the barrier of reverse step is $^{\Delta G_{2,\,orig}^{\ddagger}}$ (both are obtained by Eq. 12):

$$\Delta G_1^{\ddagger} = \max\left(min\left(\Delta G_{1,orig}^{\ddagger}, \Delta G_{2,orig}^{\ddagger}\right), \Delta G_D\right) - min\left(\Delta G_{1,orig}^{\ddagger}, \Delta G_{2,orig}^{\ddagger}\right) + \Delta G_{1,orig}^{\ddagger}$$

$$\Delta G_2^{\ddagger} = \max\left(min\left(\Delta G_{1,orig}^{\ddagger}, \Delta G_{2,orig}^{\ddagger}\right), \Delta G_D\right) - min\left(\Delta G_{1,orig}^{\ddagger}, \Delta G_{2,orig}^{\ddagger}\right) + \Delta G_{2,orig}^{\ddagger}$$

where the function max (min) selects the largest (smallest) value from the set of values in the argument of the function.

3. Derivation of Equation 3b (unproductive quenching)

First, we give an overview of the network of the relevant electron transfer reactions emphasizing the solvent cage formations.

$$\{PC^*\} + \{Q\} \underset{k_{-A}}{\overset{k_A}{\rightleftharpoons}} \{PC^* + Q\} \underset{k_{-B}}{\overset{k_B}{\rightleftharpoons}} \{PC^+ + Q^-\} \underset{k_{-D}}{\overset{k_D}{\rightleftharpoons}} \{PC + Q\} \underset{k_{-C}}{\overset{k_C}{\rightleftharpoons}} \{PC\} + \{Q\}$$

$$k_{-E} \uparrow\downarrow k_E$$

$$\{PC^+\} + \{Q^-\}$$

The lengths of the arrows indicate the expected relative rate of the forward and backward reactions based on the barrier heights. In this network the main line shows the unproductive quenching of PC* via several substeps. The $\{\mathbf{PC^+ + Q^-}\}$ caged ion-pair species is the critical branching point in this network; the vertical direction is the cage escape of the ion-pair, whereas horizontal direction to the right side is the quenching step. Figure S1, analogous with Figure 10 in the main text also shows these reactions, annotated here with the corresponding rate constants to facilitate their identification.

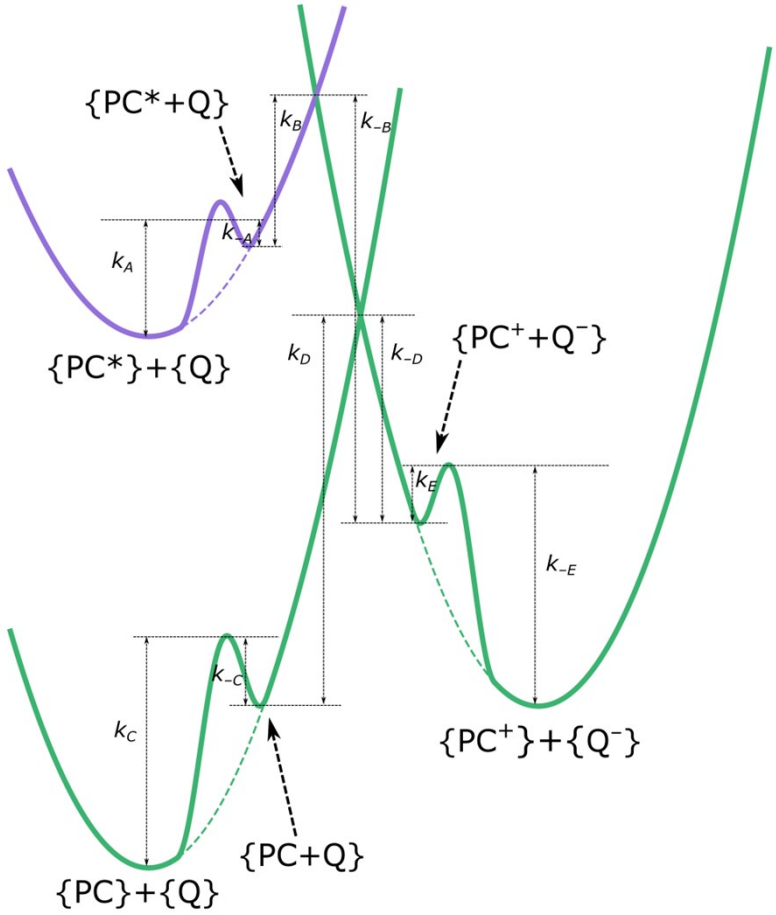

Figure S1. Marcus parabolas for the electron transfer reactions considered here, including the cage-effect. Dashed lines indicate the original parabolas. Curly brackets indicate solvated species. The energy barriers are labelled with the corresponding rate constants. For ideal case k_A, k_C and k_{-E} are equal to $k_{diffusion}$.

We can safely assume pre-equilibrium for the formation {**PC*** + **Q**$^{-}$} from {**PC*****}** + {**Q**$^{-}$} and {**PC**$^{+}$ + **Q**$^{-}$} forming from {**PC**$^{+}$} + {**Q**$^{-}$}. The cage formation might be the rate determining state only in extreme conditions, when the diffusion is hindered in a strongly viscous solvent. The pre-equilibrium condition dictates that the existence of an intermediate does not have impact on the overall rates of the forward and backward ET which can be determined from the Marcus barriers.[8] This implies that we can use a single rate constant for the consecutive reactions, if the step with highest barrier is preceded by preequilibria. This is true for the reaction route leading from {**PC***} + {**Q**} to {**PC**} + {**Q**} (unproductive quenching, see equations above), therefore it can be represented in the kinetic model with a single rate constant (k_{cr} in the main text). Note that due to the conservation law applicable to the particles, this rate constant is expressed as: $k_{cr} = (1 - \phi_{ce})k_5$.

4. Details of the kinetic simulations of the $[Ru(bpy)_3]^{2+}$ + tri-p-tolylamine (TTA) system using the COPASI software

In this simulation we used experimental data from Refs. [9] and [10]. For the fitting we have used the nanosecond transient absorption measurement of $[Ru(bpy)_3]^{2+}$ from Ref [9]; the Stern-Volmer measurement employing the photoluminescence quenching of $[Ru(bpy)_3]^{2+}$ in the presence of increasing amounts of TTA in CH_3CN and the recorded changes in absorption of TTA following the pulsed light excitation at the same concentration increments as in the photoluminescence measurements from Ref [10]. The experimental data were extracted using WebPlotDigitizer.[11] The fitted parameters were the time of the laser pulse for excitation, the concentration of $[Ru(bpy)_3]^{2+}$, a parameter to convert the strength of the laser pulse to I_p (the lamp intensity), a parameter to convert the concentration of $[Ru(bpy)_3]^{2+*}$ to emission intensity, the cage-effect yield, the lifetime (τ) of the excited state of $[Ru(bpy)_3]^{2+*}$, and k_4 and k_5. The following values were taken from the literature. Ref. [9]: $\varepsilon([Ru(bpy)_3]^{2+}, 420\ nm) = 10200\ M^{-1}cm^{-1}$; $\Delta\varepsilon([Ru(bpy)_3]^{2+}, 450\ nm) = -11000\ M^{-1}cm^{-1}$; Ref. [10]: $\Delta\varepsilon(TTA^+/TTA, 670\ nm) = 25500\ M^{-1}cm^{-1}$ Note that the first four fitted parameters were not available from the experimental details. The COPASI software offers various methods for fitting; we mainly used Genetic Algorithm but other methods yielded similar results.

The COPASI file used for the fittings as well as the files containing the experimental data were uploaded to GitHub: https://github.com/acsstirling/photokinetics/blob/main/fitting_to_exp.

5. References:

1. S. Hoops, S. Sahle, R. Gauges, C. Lee, J. Pahle, N. Simus, M. Singhal, L. Xu, P. Mendes and U. Kummer, *Bioinformatics*, 2006, **22**, 3067-3074.
2. (a) R. A. Marcus, *Annu. Rev. Phys. Chem.*, 1964, **15**, 155–196; (b) R. A. Marcus, *Angew. Chem., Int. Ed. Engl.*, 1993, **32**, 1111–1121.
3. M. D. Newton, M. V. Basilevsky and I. V. Rostov, *Chem. Phys.*, 1998, **232**, 201–210.
4. H. S. Ren, M. J. Ming, J. Y. Ma and X. Y. Li, *J. Phys. Chem. A*, 2013, **117**, 8017–8025.
5. K. K. Mentel, A. Serra, P. E. Abreu and L. G. Arnaut, *Nat. Commun.*, 2018, **9**, 2903.
6. W. Morris, E. D. Lorance and I. R. Gould, *J. Phys. Chem. A*, 2019, **123**, 10490–10499.
7. R. A. Marcus and N. Sutin, *Biochim. Biophys. Acta, Rev. Bioenerg.*, 1985, **811**, 265–322.
8. S. Kozuch and J. M. L. Martin, *ChemPhysChem*, 2011, **12**, 1413–1418.
9. A. Ripak, S. De Kreijger, B. Elias and L. Troian-Gautier, *STAR Protoc.*, 2023, **4**, 102312.
10. A. Ripak, A. K. Vega Salgado, D. Valverde, S. Cristofaro, A. de Gary, Y. Olivier, B. Elias and L. Troian-Gautier, *J. Am. Chem. Soc.*, 2024, **146**, 22818–22828.
11. A. Rohatgi, *WebPlotDigitizer*, Version 5.2, https://automeris.io.

6. Additional figures

6.1. Nonlinear dependence of the activation barrier on λ and ΔG_0

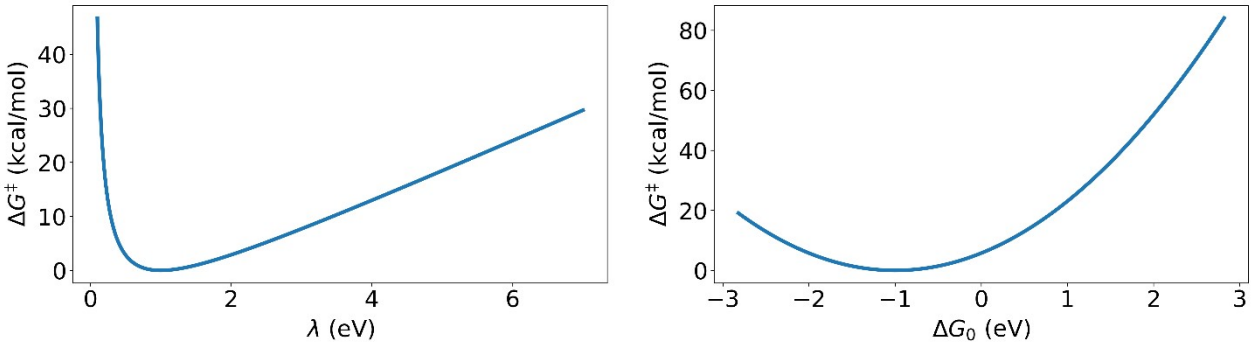

Figure S2. Nonlinear dependence of $\Delta G^{\ddagger}$ on either λ and ΔG_0 by equation $\Delta G^{\ddagger} = \frac{(\lambda + \Delta G_0)^2}{4\lambda}$ while the other parameter is fixed. Left panel: $\Delta G_0 = 1\ eV$. Right panel: $\lambda = 1\ eV$. The left panel demonstrates that both very low and very large reorganization energies can cause high ET barrier. The right panel shows that both endothermic and exothermic ETs can have significant ET barrier (in the exothermic regime this is called Marcus inverted region), whereas the minimum $\Delta G^{\ddagger}$ is reached when $\Delta G^{\ddagger} = \lambda$.

6.2. Convergence of the kinetic simulations

For all simulations, we have set a simulation time long enough (10^8 s) to ensure that the system reaches steady state. However, as Figures S3 and S4 illustrate, reaching the steady state can occur on a much shorter time-scale.

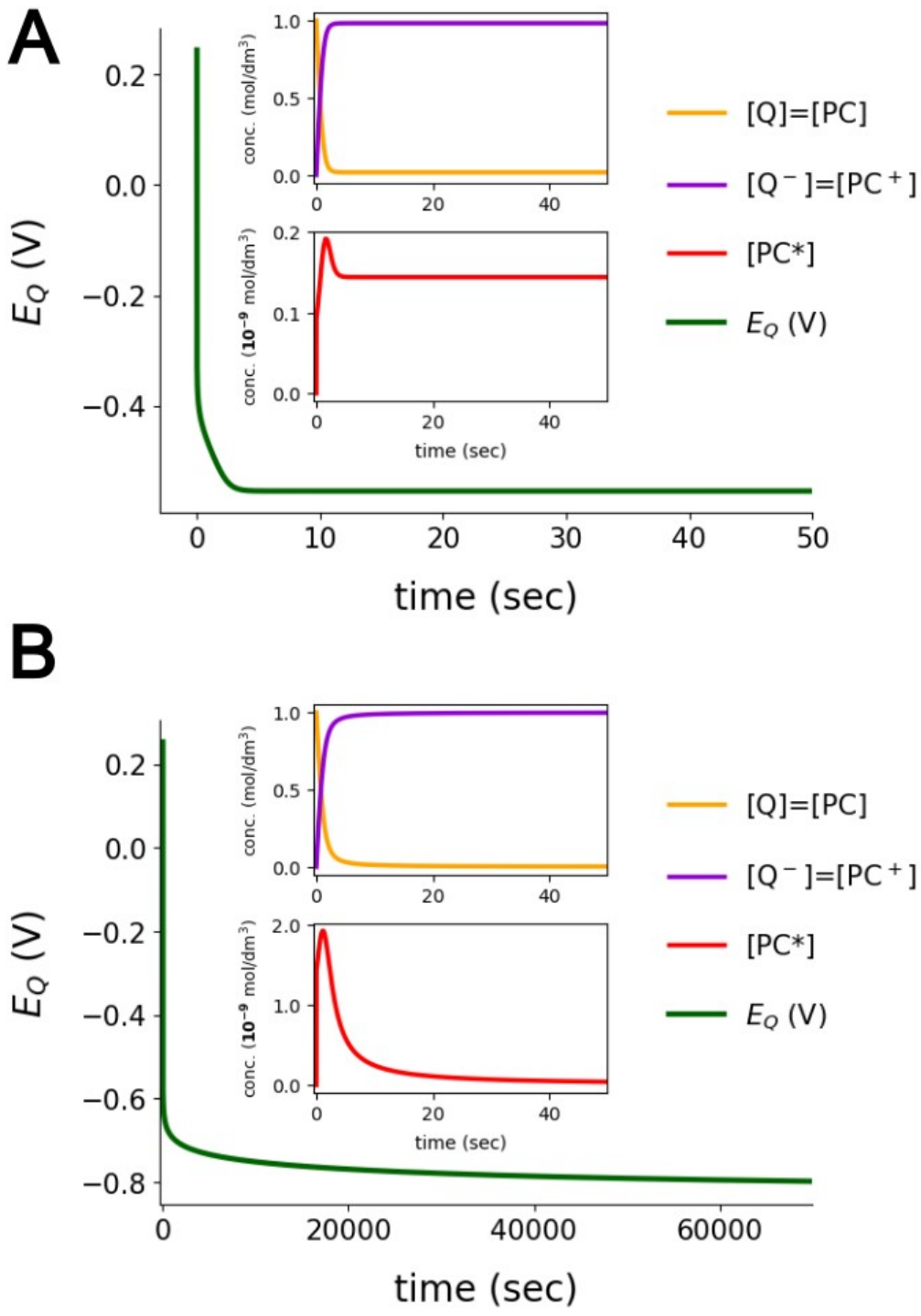

Figure S3. The panels show the time dependence of concentrations of **Q, Q**$^{-}$, and **PC***, as well as the actual reduction potential E_Q for typical setups for E_{PC}^{0} and $E_{PC^*}^{0}$. For panel A $E_{PC}^{0} = 1.5\ V$ and $E_{PC^*}^{0} = -1.5\ V$. For this pair a very fast convergence is achieved (within a few seconds). For panel B $E_{PC}^{0} = 1.9\ V$ and $E_{PC^*}^{0} = -1.75\ V$. The curves indicate that the timescale to reach the steady state is the order of a day.

To further illustrate this issue, we recalculated the 2D plot of Fig. 1 of the main text, but we set the simulation time to 24 hours (86400 s). Comparison of Fig. S4 obtained with this longer simulation time to Fig. 1 clearly shows that the differences in the predicted steady-state E_Q values are ~0.01 V at most.

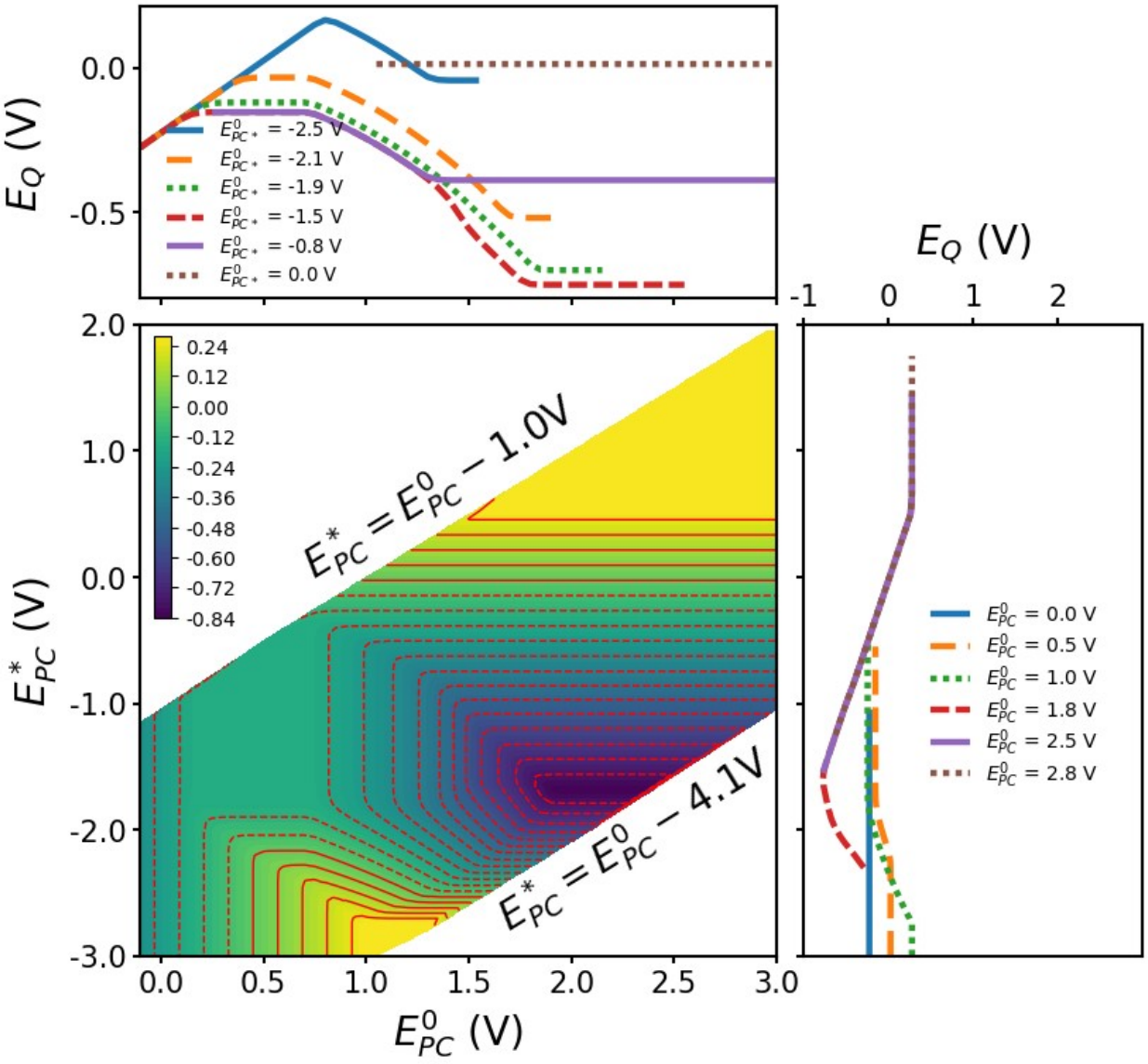

Figure S4. E_Q as a function of E_{PC}^{0} and $E_{PC^*}^{0}$ when $E_Q^0 = -0.45\ V$. The other simulation parameters are the same as in Figure 1, but the simulation time was 86400s.

6.3.Steady-state rates

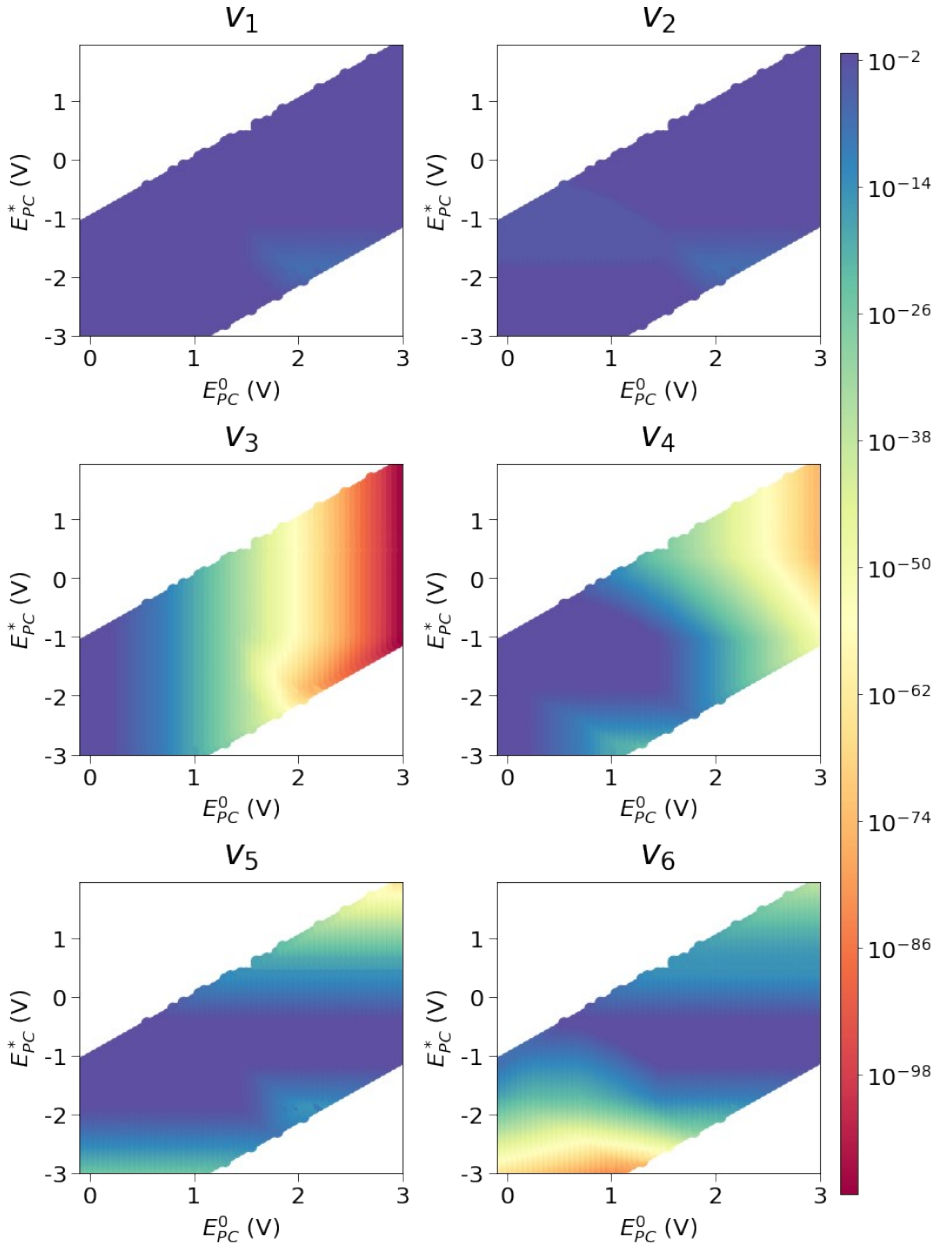

Figure S5. Steady-state rate (mol/l/s) distributions as a function of E^{0}_{PC} and E^{0}_{PC*}. The conditions are identical to those for Figure 1 in the main text. The color scale is logarithmic.

6.4. Distribution of the steady-state concentrations

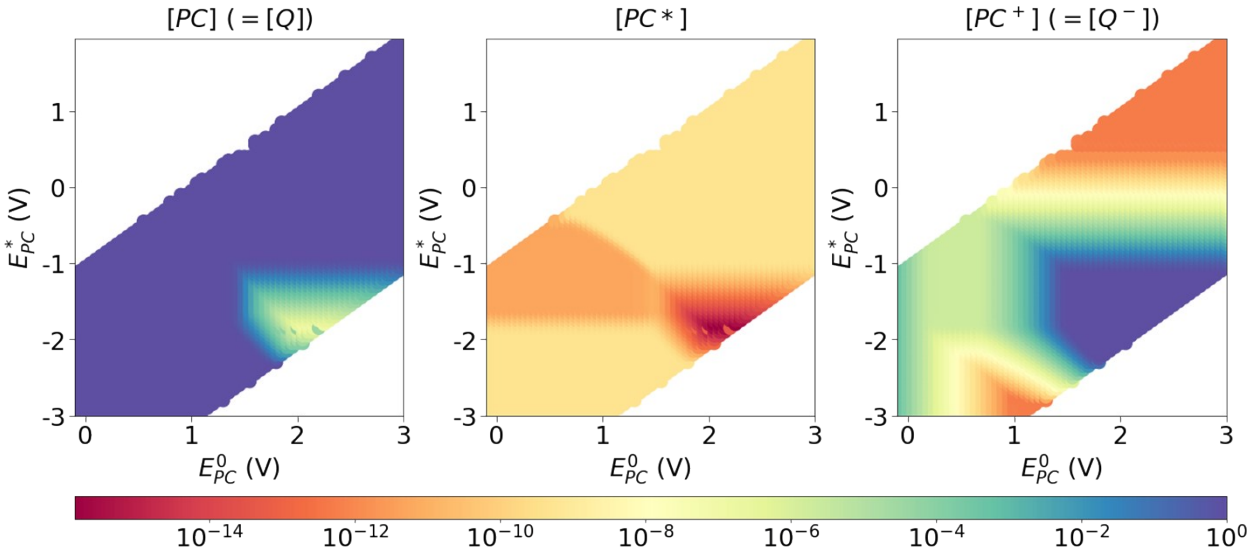

Figure S6. Steady-state concentration distributions as a function of E^{0}_{PC} and E^{0}_{PC*} in their full ranges.

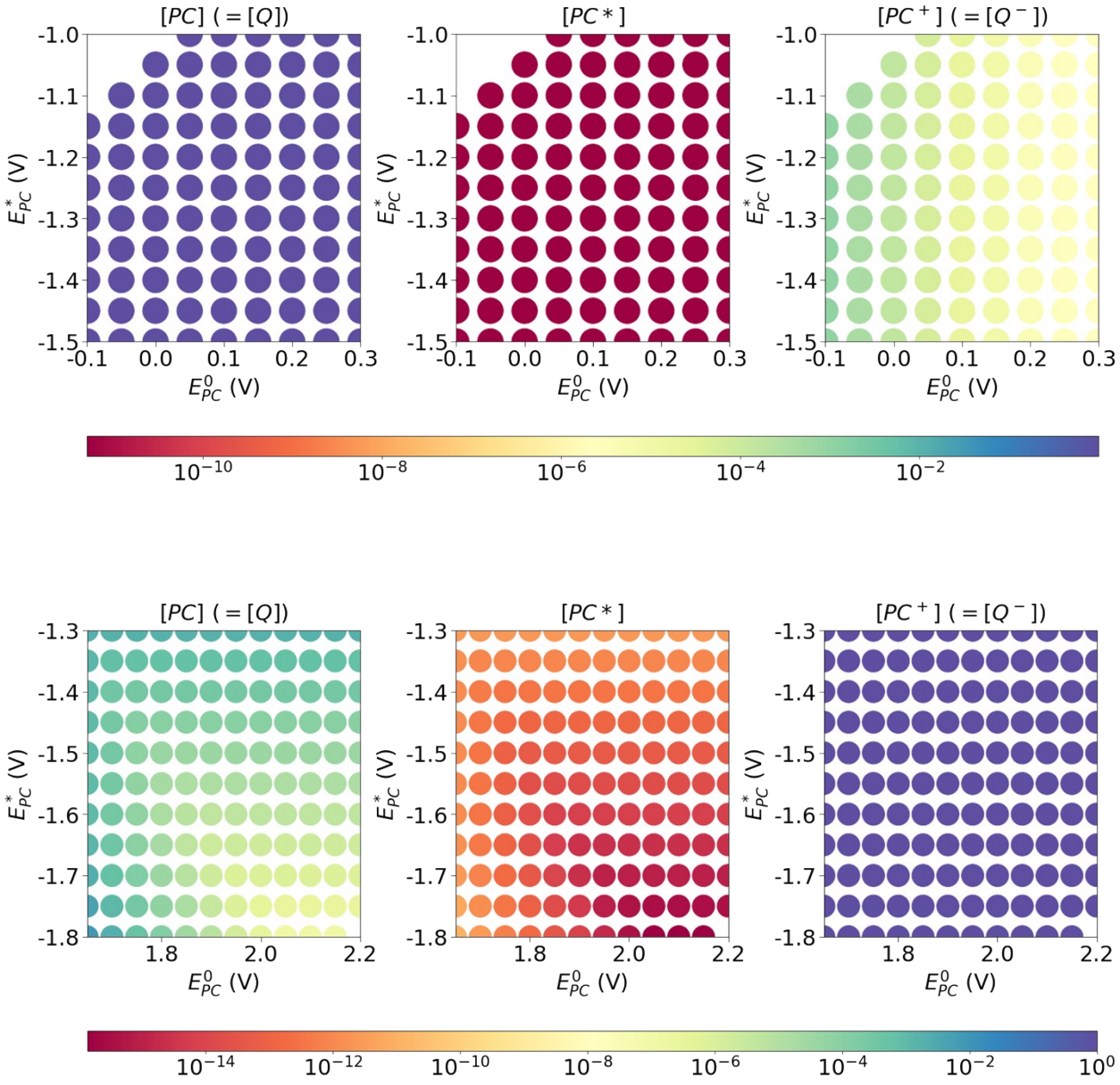

Figure S7. Stationary concentration distributions as a function of E^{0}_{PC} and E^{0}_{PC*} in their selected ranges. The circles are the simulated E^{0}_{PC} - E^{0}_{PC*} pairs, their color indicates the stationary concentration.

6.5. Distribution of E_Q for different reorganization energies

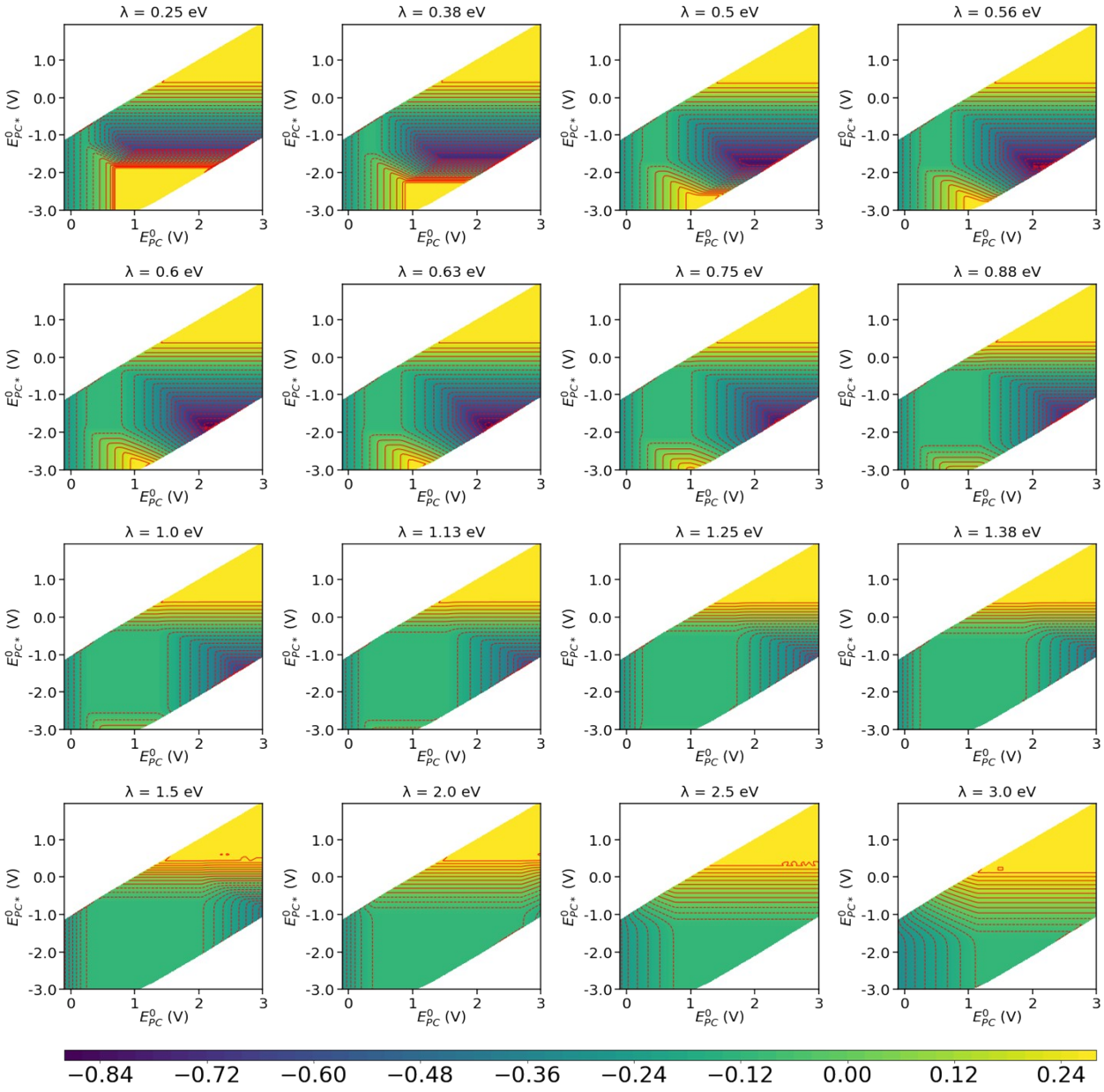

Figure S8. Distribution of E_Q as a function of $E^{\,0}_{PC}$ and $E^{\,0}_{PC*}$ for different reorganization energies (λ = 0.25-3.0 eV).

6.6. Distribution of E_Q for different lamp intensities

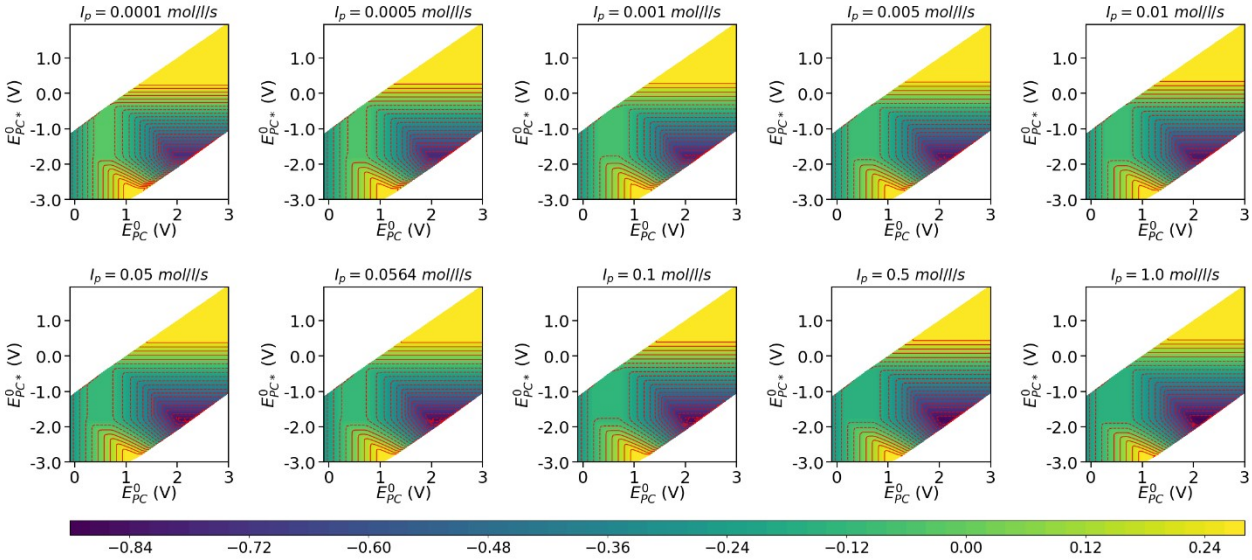

Figure S9. Distribution of E_Q as a function of $E^{\,0}_{PC}$ and $E^{\,0}_{PC*}$ for different lamp intensities (I_p = 0.0001-1.0 mol/l/s).

6.7. Distribution of E_Q for different effective absorption coefficients

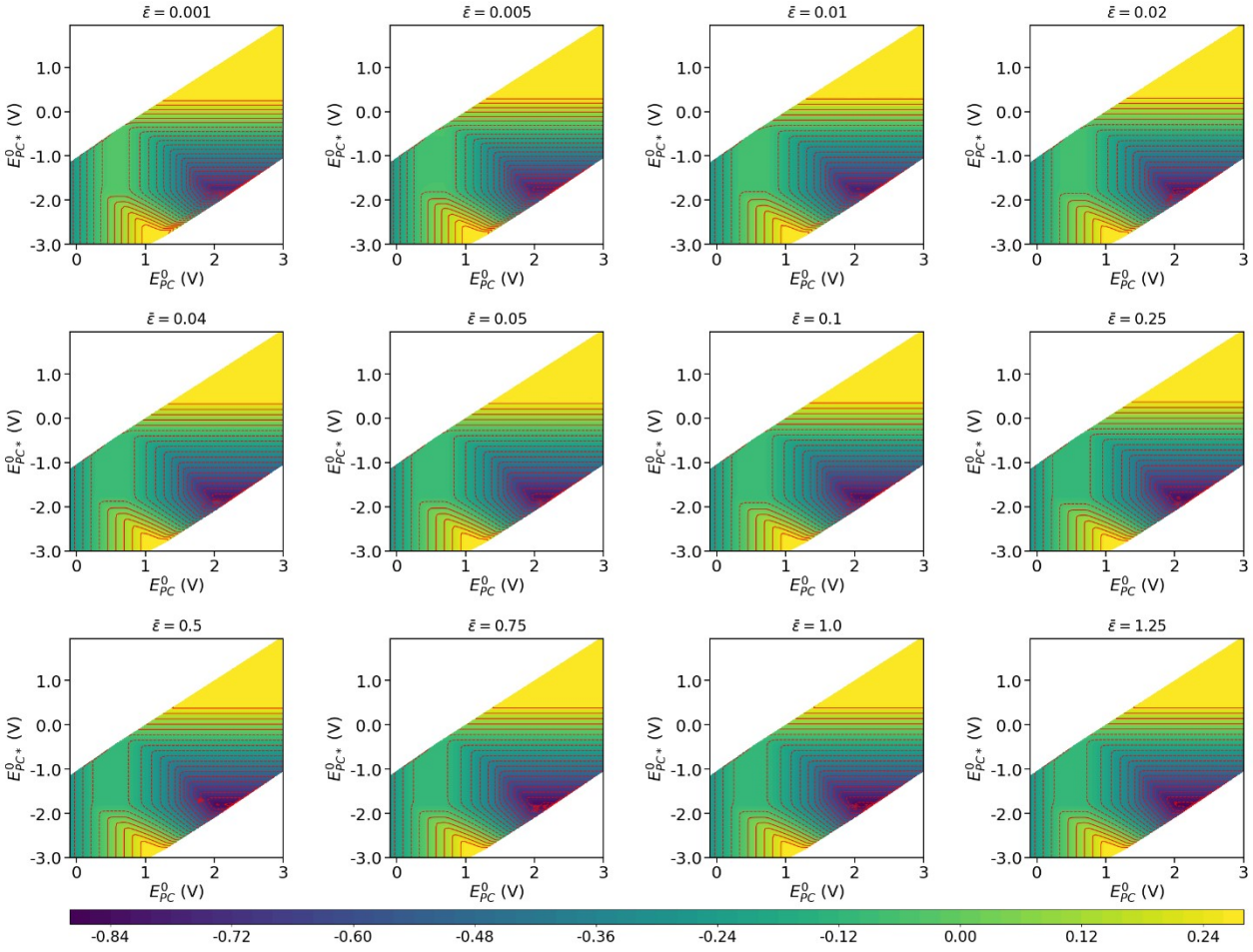

Figure S10. Distribution of E_Q as a function of E^0_{PC} and E^0_{PC*} for different effective absorption coefficients ($\bar{\varepsilon}$-s, 0.1 m^2/mol).

6.8. Distribution of E_Q for different excitation lifetimes

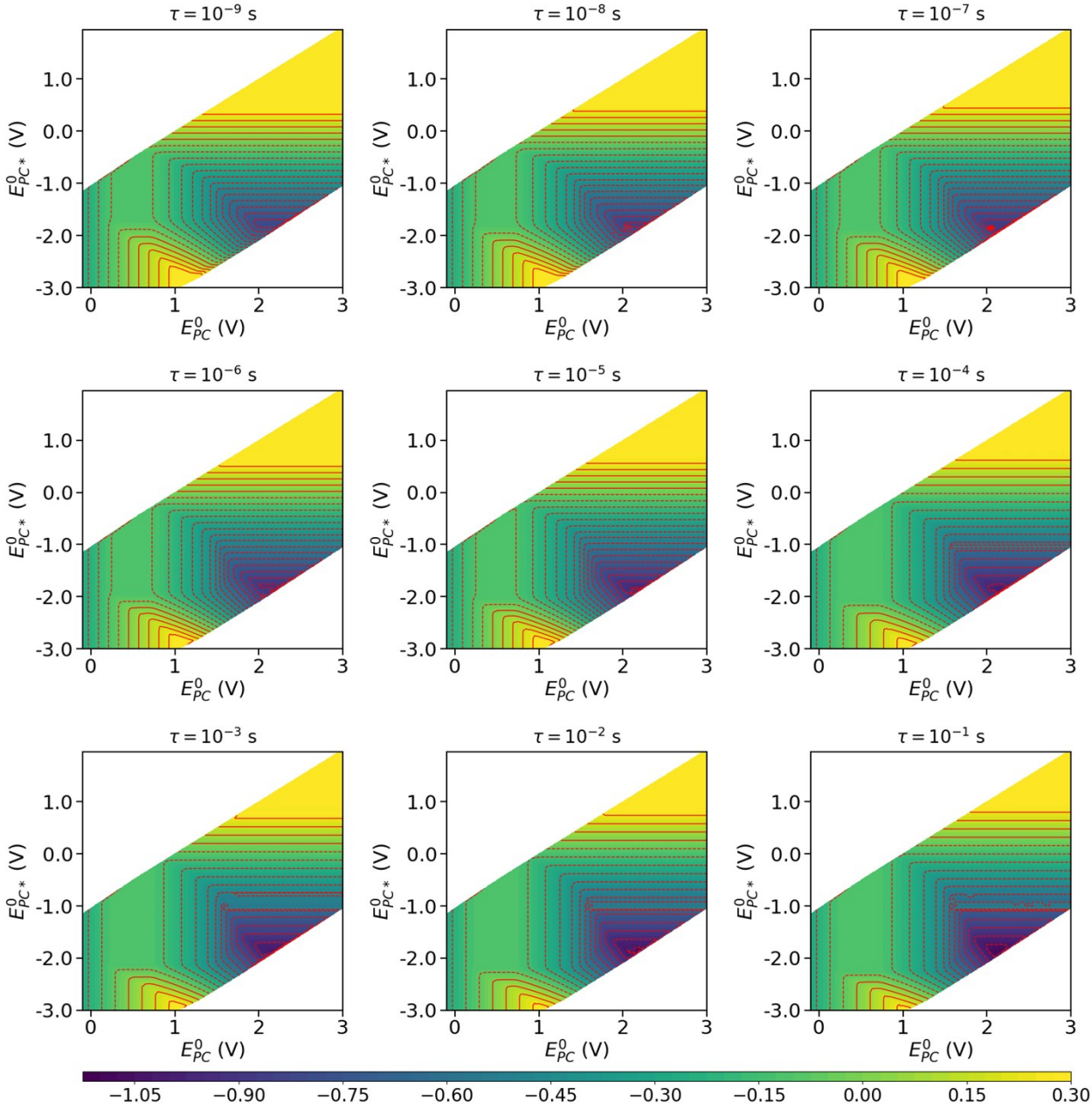

Figure S11. Distribution of E_Q as a function of E^0_{PC} and E^0_{PC*} for different excitation lifetimes ($1/k_2 = \tau = 10^{-9}$-10^{-1} s).

6.9. Distribution of E_Q as a function of E_{PC}^{0} and E_{PC*}^{0} for different diffusion rates

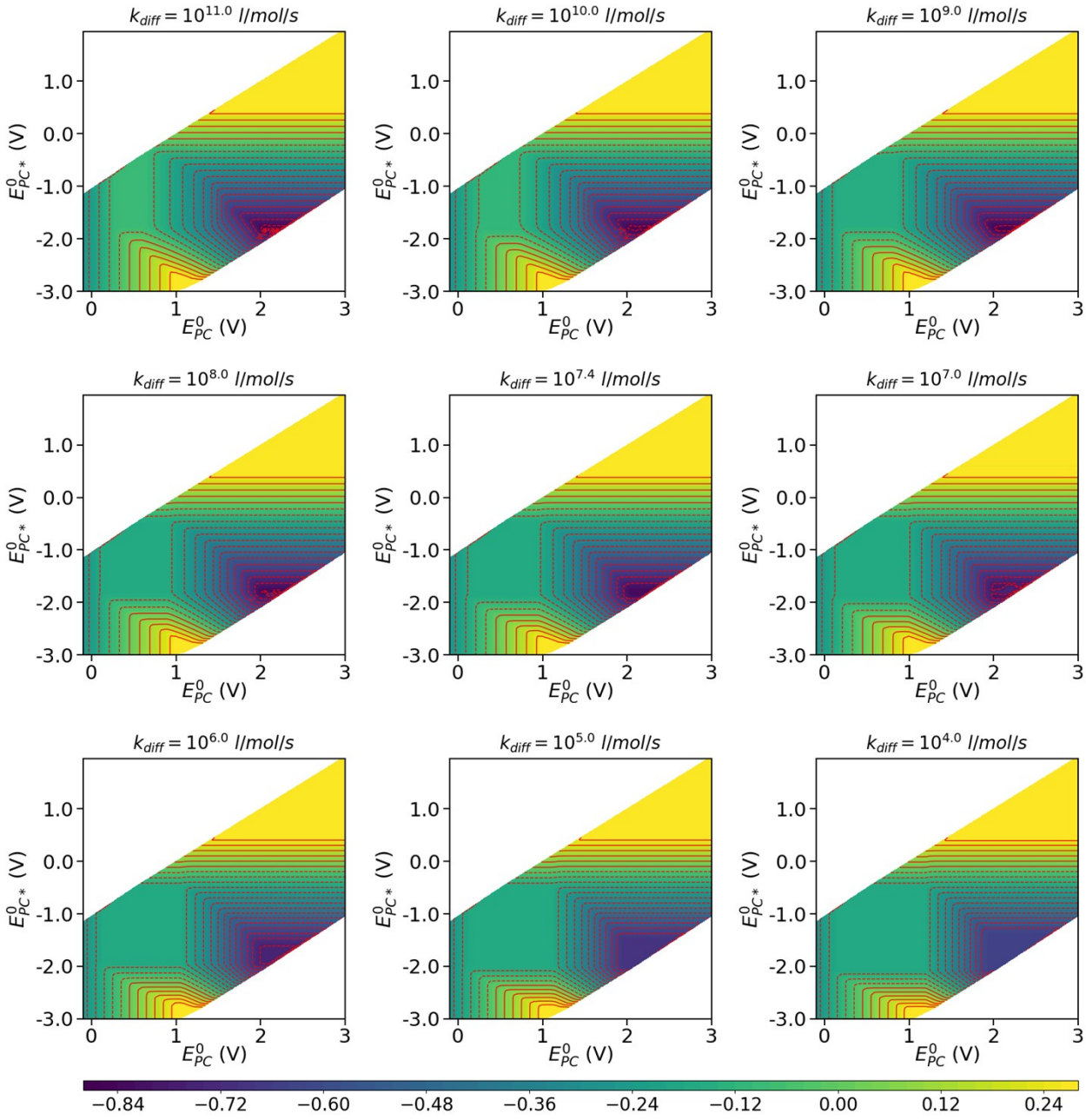

Figure S12. Distribution of E_Q as a function of E_{PC}^{0} and E_{PC*}^{0} for different diffusion rates.

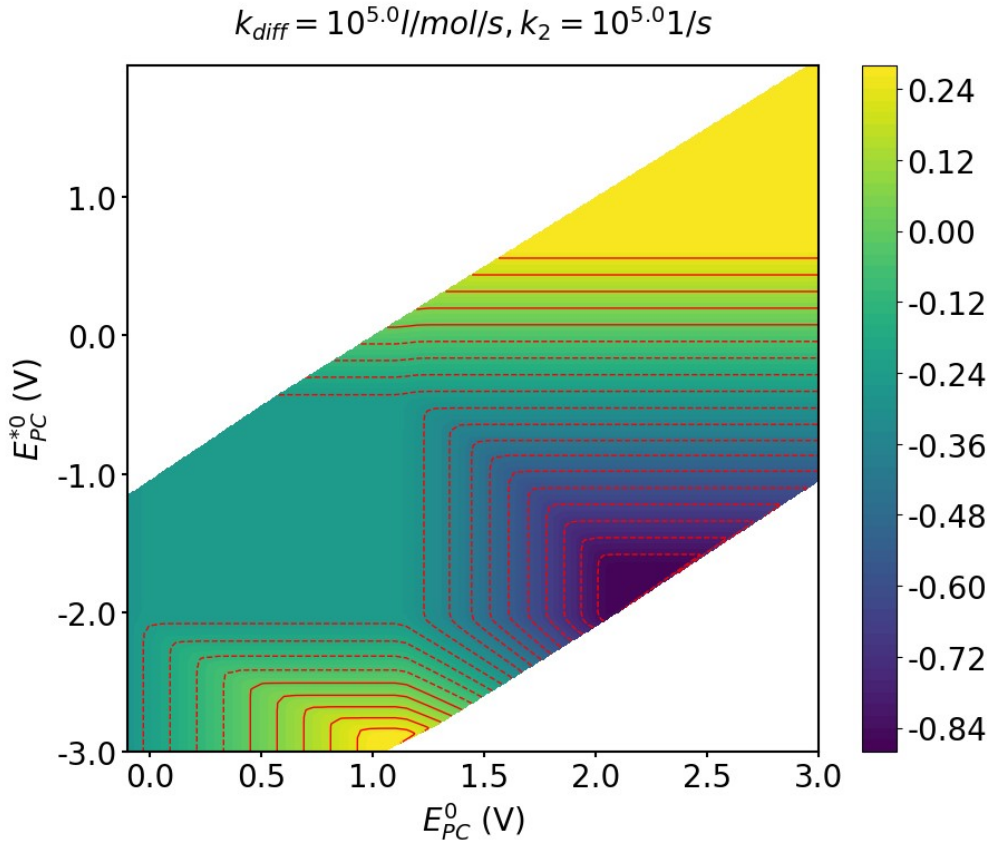

Figure S13. Distribution of E_Q as a function of E^{0}_{PC} and $E^{0}_{PC^*}$ when the rate constants of the both the diffusion limit and the deexcitation are decreased.